

Free energy simulations of single and double ion occupancy in gramicidin A

Turgut Baştuğ and Serdar Kuyucak^{a)}

School of Physics, University of Sydney, New South Wales 2006, Australia

(Received 1 November 2006; accepted 25 January 2007; published online 14 March 2007)

Simultaneous occupancy of the two binding sites in gramicidin A by monovalent cations is a well known property of this channel, but the energetic feasibility of this process in molecular dynamics simulations has not been established so far. Here the authors study the energetics of single and double ion occupancy in gramicidin A by constructing the potential of mean force for single and pair of cations. As representatives of small and large ions, they consider both Na⁺ and K⁺ ions in the calculations. Binding constants of ions are estimated from the free energy profiles. Comparisons with the experimental results indicate 3–4 kT discrepancy in the binding energies. They also study the coordination of the ions in their respective binding sites and the dynamic behavior of the channel water during the double ion binding process. © 2007 American Institute of Physics.

[DOI: 10.1063/1.2710267]

I. INTRODUCTION

Most ion channels are occupied by multiple ions, which is of crucial importance for enabling fast permeation while maintaining a strict selectivity. The crystal structure of the KcsA potassium channel has provided a lucid example of how nature has achieved this feat in practice.^{1–3} The same principle is employed in many other biological ion channels where selective permeation is essential. Typically ions are attracted to a binding site which works as a selectivity filter. The potential well at the binding site is usually quite deep so that a single ion would be permanently bound there. However, the presence of multiple ions and the repulsive Coulomb interaction among them plays a destabilizing role, thus facilitating fast permeation.

The gramicidin A (gA) channel deviates from this script common to most biological ion channels in important ways. The binding sites at either end of the channel are energetically just deep enough to hold a single monovalent cation. Thus at low concentrations, when the probability for simultaneous occupation of both binding sites is quite low, gA functions as a single ion channel (for reviews of the physiology of the gA channel, see Refs. 4 and 5). At higher concentrations though, both binding sites in the channel can be occupied by monovalent cations. Because the binding sites are well separated (~ 20 Å) by a single-file column of water, the role of Coulomb repulsion in permeation is marginal. The weaker ion-channel and ion-ion interactions, coupled with the simplicity of the gA structure, confer the gA system a distinct advantage for testing theoretical models of ion channels. Discrepancies that would be hard to detect in biological ion channels due to the overwhelmingly large Coulomb interactions among the ions and charges in the channel protein could be more easily detected in the more benign environ-

ment of gA. Thus the gA channel continues to play an important role in testing the methods and models employed in the description of ion channels.

The structure of gA has been known for a long time—the initial left-handed β -helical dimer model proposed by Urry⁶ was later refined (shown to be right handed) using solution⁷ and solid state NMR.⁸ At present there are two high-resolution structures of gA that are commonly used in computational studies, namely, PDB:1MAG (Ref. 9) and PDB:1JNO.¹⁰ In the absence of any other channel structure, gA had been seen as a prototype ion channel and extensively studied using various computational methods (for reviews see Refs. 11–14). Due to insufficient computational power, initial models of gA attempting to account for its conductance tended to be more phenomenological, and when microscopic methods such as molecular dynamics (MD) simulations were employed, comparison of their predictions with the permeation properties of gA was rather limited. The recent demonstration of the breakdown of continuum electrostatics in the gA channel^{15,16} has ruled out application of phenomenological models that rely on continuum solutions of the Poisson equation, which put further pressure on application of microscopic simulation methods to gA. Fortunately developments in cluster technology have improved the time impasse faced by MD simulations, and already several MD studies of the permeation properties of the gA channel have appeared in literature.^{17–21} So far the focus of all these studies has been permeation of a single K⁺ ion, and the energy barrier it faces at the center of gA, though Ca²⁺ and Cl⁻ ions are also considered more recently.²¹ In the face of all the available data in gA, this is quite a limited application of the MD method. The study of other monovalent cations, organic cations,²² and especially double ion occupancy of gA would provide valuable complementary information.

The experimental evidence for double occupancy of gA is wide and varied. For the larger cations (e.g., K⁺, Rb⁺, and Cs⁺), double occupancy was inferred from saturation of

^{a)}Electronic mail: serdar@physics.usyd.edu.au

channel currents^{23–27} and tracer flux ratio measurements.^{28–30} Double occupancy of the smaller Na⁺ and Li⁺ ions is less probable and therefore harder to establish from flux measurements alone. Initial indication for double occupancy of Na⁺ came from streaming potential measurements.^{31,32} Solid evidence for double occupancy of all alkali metal cations was eventually obtained from NMR experiments.^{33,34}

There have been very few theoretical studies of double ion occupancy in gA.^{35,36} In the only MD study,³⁶ the free energies for single and double occupancy were calculated for Na⁺ ions, and the double occupancy free energies for other ions relative to that of Na⁺ were determined using the free energy perturbation method. The free energies of binding for single and double Na⁺ ions were found to be +2 and +8 kcal/mol, respectively. That is, a pair of Na⁺ ions did not bind to gA, but more surprisingly even a single Na⁺ ion could not bind to gA. This discrepancy may be due to insufficient sampling arising from limited computational time. The relative free energies of double occupancy, on the other hand, being less susceptible to such errors, were found to be consistent with the experimental observations. Namely, the double occupancy of gA was more probable for the larger ions relative to the smaller ones. The problem with the binding of Na⁺ ion to gA was considered in a later paper,³⁷ but neither the position of the binding site nor the free energy of binding could be satisfactorily explained.

It is clear from the above review that double ion occupancy and Na⁺ ion binding remain as outstanding problems for MD simulations of the gA channel. Here we address these problems by constructing the potential of mean force (PMF) for K⁺ and Na⁺ ions, both singly and as a pair. For this purpose we use both umbrella sampling and steered MD simulations. The binding constants for single and double occupancy of gA are estimated from the respective PMF's and compared to the results with the available experimental data. We also study the coordination of the ions in their respective binding sites and the dynamic behavior of the channel water during the double binding process.

II. METHODS

A. Model system and MD simulations

In previous MD simulation of the gA channel,^{17,20,21} we employed the 1MAG structure for the gA dimer⁹ with 48 lipids per layer. Here we wish to carry out longer MD simulations of the system in order to check the convergence of the results. Reducing the number of lipids is an obvious way to achieve this, e.g., ten lipids per layer have been suggested to be adequate.³⁸ Also we employ the 1JNO structure for gA,¹⁰ which has been shown to relax to equilibrium faster.³⁸ To determine the optimal number of lipids, we have constructed several model systems using the VMD suit of software.³⁹ Initially a bilayer of dimyristoylphosphatidylcholine molecules with 128 lipids per layer is constructed and the 1JNO structure of gA (Ref. 10) is embedded in the middle of this system. The lipids at the periphery of this system are gradually removed—while preserving a rectangular shape—to obtain four systems with 64, 32, 16, and 10 lipids per layer. During the initial phase, the gA atoms are constrained to their initial

positions. Each system is hydrated with about 50 water molecules per lipid and placed in an orthorhombic periodic box. Following an energy minimization of 10 000 steps, they are equilibrated with surface-tension coupling until the surface area converged to the experimental lipid density of 60 Å² per lipid.⁴⁰ In the remaining simulations, the periodic box is fixed in the *x* and *y* directions and a pressure coupling of 1 atm is applied in the *z* direction. At this stage, a number of water molecules are replaced with K⁺ and Cl⁻ ions so that the solution has the physiological concentration of about 150 mM. The restraints applied to the gA atoms are then gradually relaxed in MD simulations lasting 2 ns, followed by 1 ns equilibration. To test the suitability of these systems for free energy simulations, we have calculated the free energy of translocating a K⁺ ion to the gA center using thermodynamic integration.⁴¹ For the systems with 16, 32, and 64 lipids per layer, the calculated free energies are found to converge, exhibiting minimal hysteresis, but a large hysteresis effect is observed in the system with ten lipids. Therefore, in the present work we have used the gA system with 16 lipids per layer. The dimensions of this system in the *x*, *y*, and *z* directions are 38, 32, and 72 Å, and it contains 1540 water molecules with four pairs of KCl ions.

MD simulations are carried out using the NAMD code, Version 2.5 (Ref. 42) with the PARAM27 version of the CHARMM force field,⁴³ which provides a complete set of parameters for all the atoms in the system and uses the TIP3P water model. An *NpT* ensemble is used with periodic boundary conditions. The pressure is kept at 1 atm using the Langevin piston method with a damping coefficient of 5 ps⁻¹.⁴⁴ Similarly, temperature is maintained at 298 K through Langevin damping with a coefficient of 5 ps⁻¹. Electrostatic interactions are computed using the particle-mesh Ewald algorithm. The list of nonbonded interactions is truncated at 13.5 Å, and a switching cutoff distance of 10 Å is used for the Lennard-Jones interactions. A time step of 2 fs is employed in all simulations. Trajectory data are written at 1 ps intervals during both equilibration and production runs.

B. Potential of mean force and binding constants

The PMF of K⁺ and Na⁺ ions along the gA channel axis is calculated using umbrella sampling⁴⁵ together with the weighted histogram analysis method (WHAM).⁴⁶ As the method was explained in some detail earlier,^{17,20} we give a brief account here stressing only the differences in the present work. Using an umbrella potential, we sample an ion's position at equal intervals along the channel axis during MD simulations of the system. The biased ion distributions obtained from the production runs are then unbiased and combined using WHAM. In all cases, the ion coordinates are measured with respect to the center of mass of gA. We find that due to fluctuations in the system, the equilibrated structures do not exhibit a clear symmetry around *z*=0, which is also reflected in the calculated PMF's. One way to deal with this problem is to use the symmetrized ion densities in the construction of the PMF,^{18,19} i.e., $\rho_{\text{sym}}(z) = [\rho(z) + \rho(-z)]/2$, which we also adopt here.

We employ umbrella potentials with a force constant of

10 kcal/mol/Å² at 0.5 Å intervals. Outside the pore ($z > 11$ Å), where the changes in the PMF are smaller, the force constant is reduced to 7 kcal/mol/Å² to improve the overlap of ion distributions between neighboring windows. For $z > 15$ Å, an additional biasing potential with a force constant of 1 kcal/mol Å² is applied in the radial direction to prevent large excursions of the ion from the central axis. Comparison of the PMF results with and without a radial constraint indicates a negligible shift in energy. To avoid potential equilibration problems associated with dragging of an ion in the channel, we have replaced individual water molecules in the pore with a K⁺ ion.^{18,20} This way we obtain ten configurations with the ion placed at regular intervals along the channel axis. The K⁺ ion in each configuration then needs to be pushed by at most 1 Å to either side in order to generate the full set of windows required in the PMF calculations. Outside the channel, where equilibration is not a problem, the ion is pushed along the central axis. A total of 81 windows covering the range $[-20, 20]$ Å are employed for the single ion PMF's. For the K⁺ PMF, the system is equilibrated for 200 ps and the trajectory data for ion positions are collected for 1.5 ns for each window. The simulation systems for the Na⁺ PMF are obtained from those for the K⁺ PMF by substituting all the K⁺ ions with Na⁺. The simulation system for each window is then equilibrated for 0.7 ns, followed by a 1 ns production run.

The construction of the double ion PMF is not as straightforward as in the single ion case. An obvious method is to put the first ion in one of the binding sites and construct a PMF for the second ion on the other side. However, during a 0.5 ns per window simulation of this process, the bound ion is observed to leave the binding site when the second one approaches the other binding site. A simple way to deal with this problem is to apply a small restraining force on the bound ion to prevent it from leaving the binding site. We have found that a minimal 2 kcal/mol Å² harmonic restraint is adequate for this purpose. A more suitable method in such a nonequilibrium situation is to use Jarzynski's equality⁴⁷ in steered MD (SMD) simulations.⁴⁸ Here a harmonic force is applied to an ion in bulk via a stiff spring, whose reference point is pulled to the binding site along the z axis at a constant velocity v , i.e., $z_{\text{ref}}(t) = z_0 + vt$. For each SMD path, the work done W is calculated from the integral of the force on the spring, and the free energy change is determined from the ensemble average of the work done for several SMD paths as $e^{-\beta\Delta F} = \langle e^{-\beta W} \rangle$, where $\beta = 1/k_B T$ is the inverse temperature. In SMD simulations, we use a spring constant of $k = 20$ kcal/mol Å² and a pulling velocity of $v = 2.5$ Å/ns. PMF is determined from the average of ten SMD trajectories. Tests involving steering of an ion over a Gaussian barrier indicate that these parameters are adequate for reproducing the potential energy profile. For comparison, we consider both umbrella sampling and SMD methods in PMF calculations for the binding of a second K⁺ ion to gA.

An alternative method that is especially suitable for finding the binding sites for double occupancy and analyzing their structure at equilibrium is to move the ions symmetrically so that they are bound to the channel simultaneously. The umbrella potential for the two ions is taken as

$$U = \frac{k}{2} [(z_1 - z_{10})^2 + (z_2 - z_{20})^2], \quad (1)$$

where z_1 and z_2 refer to the ion positions and z_{10} and z_{20} are the window positions. The windows are placed symmetrically by setting $z_{10} = Z_0 - z_0$ and $z_{20} = Z_0 + z_0$, where Z_0 refers to the gA center of mass and $2z_0$ is the distance between the two windows. We use a similar transformation for the ion coordinates, i.e., $z_1 = Z - z$ and $z_2 = Z + z$, where Z is the center of mass of the two ions and $2z$ is the distance between them. Substituting the above values of ion positions in Eq. (1), the umbrella potential can be written as

$$U = k(Z - Z_0)^2 + k(z - z_0)^2. \quad (2)$$

Equation (2) shows that, taking half the distance between the ions as the reaction coordinate, the two-ion PMF can be unbiased just like in the case of a single ion PMF (but with an increased force constant).

Simulation systems for the double ion PMF are constructed in a manner similar to the single ion case. Two K⁺ ions are placed at the binding sites at $z = \pm 11$ Å, and the system is equilibrated for 0.7 ns while the ions are restrained with the usual umbrella potentials. The ions are then moved simultaneously in 0.5 Å steps to $z = \pm 16$ Å and to $z = \pm 9.5$ Å, generating a total of 14 windows. The system is equilibrated for 0.7 ns at each window. The initial system has seven water molecules in the pore but one of the water molecules escapes when the ions are pushed in beyond ± 10 Å. The PMF is calculated from a 1 ns production run for each window. The simulation systems for Na⁺ are again obtained from those of K⁺ by substitution followed by 0.7 ns equilibration for each window. Because Na⁺ can go further into the channel, an additional window at $z = \pm 9$ Å is included in the PMF calculation.

Accuracy of the one-dimensional (1D)-PMF calculations in the bulk region is checked via independent free energy calculations using the thermodynamic integration method. In this method, the free energy difference is obtained from

$$\Delta G = \int_0^1 \left\langle \frac{\partial H(\lambda)}{\partial \lambda} \right\rangle_{\lambda} d\lambda, \quad (3)$$

where $H(\lambda) = (1 - \lambda)H_0 + \lambda H_1$, with H_0 and H_1 representing the Hamiltonians of the initial and final states, respectively. Here the initial state is taken as a K⁺ ion in the bulk and a water molecule in the binding site of gA, and in the final state these two are interchanged. In order to reduce fluctuations in the free energy calculations, we perform the alchemical transformation via an intermediate state with no charge, which we choose as a water molecule with the partial charges set to zero (denoted as W_0). Thus we perform two calculations, $\Delta G(K^+ \rightarrow W_0)$ and $\Delta G(W_0 \rightarrow W)$, whose sum gives the desired free energy change for the $K^+ \rightarrow W$ transformation. Note that a similar transformation, $W \rightarrow W_0 \rightarrow K^+$, is carried out in the binding site simultaneously to find the ionic free energy difference between the channel and bulk water. The integral in Eq. (3) is performed using a Gaussian quadrature with seven points, which has been found to be sufficiently accurate.²¹ The system is equilibrated

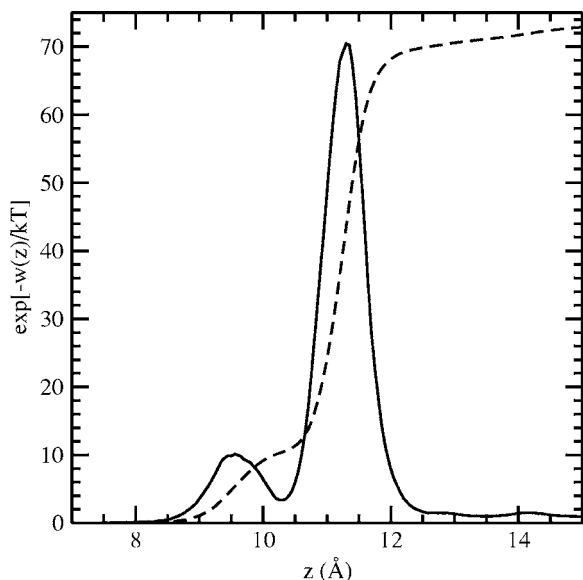


FIG. 1. The value of the integrand in Eq. (4) along the channel (z) axis (solid line), and the result of the integral for the interval $[0, z]$ (dashed line), obtained using the PMF of a K^+ ion given in Fig. 2(b).

for 200 ps and the integrals are evaluated from 1 ns of production runs.

Binding constant of an ion can be estimated from the integral of the PMF, $W(r)$ in the vicinity of the pore

$$K = \int_{\text{pore}} e^{-[W(r)-W_0]/kT} dr, \quad (4)$$

where W_0 is the reference value of the PMF in bulk, which is set to zero in practice. The exponential function in Eq. (4) has very large values in the binding site and remains relatively small outside. This is demonstrated in Fig. 1, which shows the values of the integrand for the PMF of a K^+ ion given in Fig. 2(b), and its integral from 0 to z (solid and dashed lines, respectively). The major contribution to the integral is seen to come from the binding site, which covers the range of 9–12 Å. Further, in the binding site the ion's off axis motion is quite restricted. The PMF steeply rises beyond 2–3 Å due to the repulsive Lennard-Jones forces from the peptide atoms, and again any contribution to the integral beyond that range is negligible. Thus, to a good approximation, the integral in Eq. (4) can be evaluated using a 1D-PMF

$$K = \pi R^2 \int_{z_1}^{z_2} e^{-W(z)/kT} dz, \quad (5)$$

where R is an effective radius for the ion in the binding site, which can be determined by sampling the radial position of the bound ion during MD simulations. The integration limits z_1 and z_2 are chosen in the bulk region where W vanishes. For the present PMF's, an adequate choice is ± 15 Å (choosing a larger value gives essentially the same result). The above approximation is quite reasonable when other factors affecting the calculation are considered, e.g., a typical 1 kT uncertainty in the PMF translates to a factor of 3 uncertainty in the binding constant.

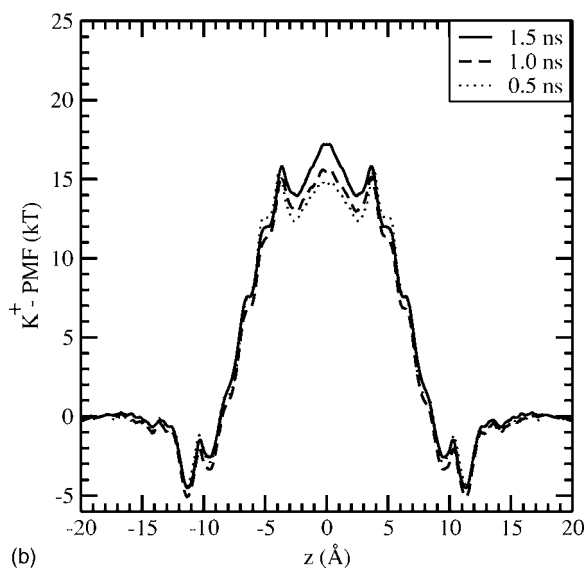
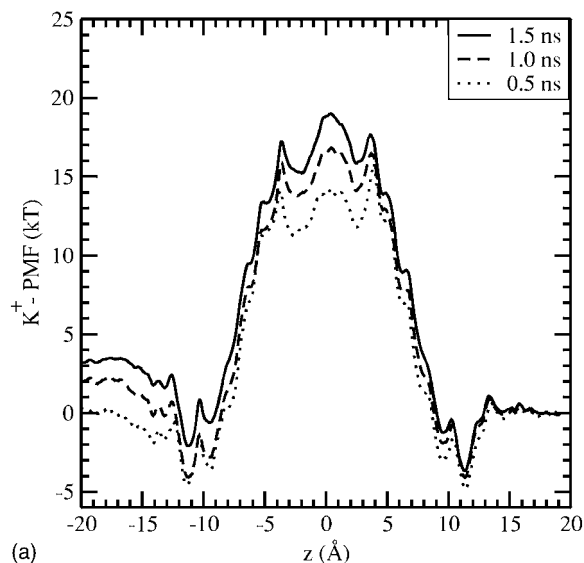


FIG. 2. PMF profiles of a K^+ ion along the central axis of the gramicidin A channel obtained using the raw ion densities (A) and the symmetrized ones (B). The ion density is symmetrized using $\rho_{\text{sym}}(z)=[\rho(z)+\rho(-z)]/2$. The dotted, dashed, and solid lines show the PMF obtained from 0.5 ns, 1 ns, and 1.5 ns MD simulations for each window.

III. RESULTS AND DISCUSSION

In presenting the single and double ion PMF's, we do not apply any correction factors arising from the system size and lipid polarization, which have been estimated from continuum methods in previous work.^{18,19} Our purpose here is to test the predictive power of MD force fields, and such corrections should ideally be calculated within the MD framework to be reliable. For example, we have studied the finite size effect on the free energy barrier of ions in gA by systematically increasing the system size in MD simulations. We have calculated the free energy barrier at the center of the channel with respect to the bulk solution using the thermodynamic integration method.⁴⁹ Our results indicate no significant change—the energy barrier increases by 1 kT, which is the accuracy limit of the calculations. This result is to be contrasted with the continuum estimate of the finite size effect, which predicted a decrease in the barrier height by

-2.7 kT.¹⁸ The second effect considers corrections for the neglected polarization interaction from continuum electrostatics, but only for the lipid molecules. As pointed out before,⁵⁰ a self-consistent treatment of the polarization interaction is very important, and a partial incorporation of polarizability may introduce even larger errors than completely neglecting it. Thus a fully polarizable MD force field is required for assessing the effect of the polarization interaction on the energetics of ion permeation. We also note that these effects are shown to be most important when the ion is at the center of the channel but they become negligible at the binding site and outside,¹⁸ which is the main focus of this study.

A. Potential of mean force of ions

Due to large system size, we could not properly address convergence issues in previous PMF calculations of K^+ ions in gA.^{17,20} Using a smaller system has allowed us to run much longer simulations so that convergence of the PMF can be studied. We choose the K^+ ion PMF for this purpose as in the previous studies to provide a justification for them as well. We have extended the MD simulations up to 1.5 ns for each window in the construction of the K^+ PMF. To study the convergence of the results, we construct three PMF's using the trajectory data from the simulation intervals, 0–0.5, 0–1, and 0–1.5 ns. In Fig. 2(a), the PMF's obtained using the raw ion densities are shown. There is a few kilotesla asymmetry between the left and right sides of the PMF's, and most of the contributions to the asymmetry come from the periphery of the binding sites. There is no clear convergence pattern even after 1.5 ns simulation, which suggests that the asymmetry in the PMF is due to slow fluctuations in the system and will require much longer simulations to converge to a symmetric profile. An obvious source of this asymmetry is the slow fluctuations of the gA center of mass with respect to the lipid bilayer (up to an angstrom). Indeed, the gA center of mass nearly coincides with the bilayer one in the initial PMF but it is observed to drift upwards relative to the bilayer in subsequent PMF's, which is consistent with the increase of asymmetry in the PMF, Fig. 2(a). Such a drift is seen to lead to asymmetries in the carbonyl orientations, especially those of Leu10, Leu12, and Leu14, which point out of the channel and hence do not make stabilizing hydrogen bonds with the other residues. These leucine residues play an important role in the binding of ions, thus asymmetries in their orientations lead to asymmetries in the PMF.

Because much longer MD simulations are not feasible even with this smaller system, we use the symmetrized ion densities to remedy this problem.¹⁸ As shown in Fig. 2(b), the symmetrized PMF's have converged to within 1 kT everywhere except the central part. Fluctuations at the center where the two gA monomers are linked are much larger which explains the slower convergence of the PMF there. Otherwise, the results in Fig. 2(b) demonstrate that using symmetrized ion densities, a reliable PMF can be obtained from 0.5 ns MD simulations, which justifies earlier K^+ PMF's.

A second issue is the validity of the above 1D-PMF results in the bulk region. Because the ion is free to move off

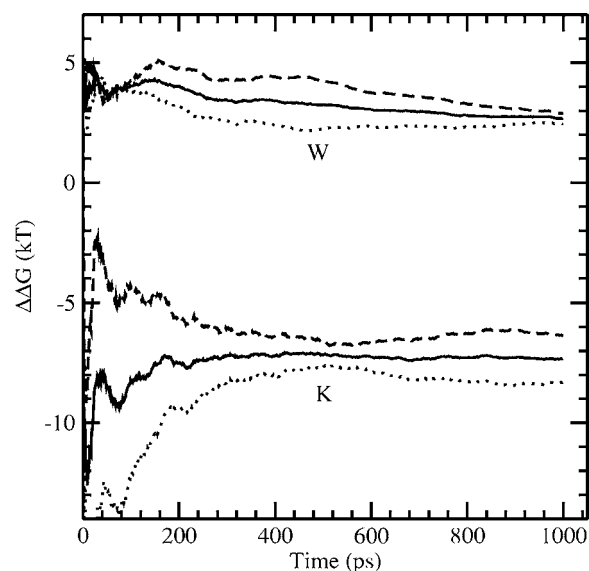


FIG. 3. Running averages of the free energy differences ΔG_+ (dashed line) and $-\Delta G_-$ (dotted lines) for transferring a K^+ ion from bulk to the binding site of gA and the reverse process, respectively. The curve labeled K shows the $K^+ \rightarrow W_0$ leg of the transformation, and W shows the $W_0 \rightarrow W$ leg. For each leg, ΔG is obtained from the average of the two curves and depicted with the solid lines. The total free energy is obtained by adding the end points of the solid lines.

axis in bulk, this may cause the 1D-PMF to diverge in long simulations. Our simulations are relatively short and the ion remains in the vicinity of the central axis during the PMF calculations. Thus we expect the 1D-PMF to be quite a reasonable approximation. This is supported by the convergence of the PMF to a flat value outside the channel. Nevertheless there may still be an offset in the calculated bulk free energy due to the 1D approximation, which needs to be checked. We have recently tested the validity of the 1D-PMF results by comparing them with independent free energy calculations obtained from thermodynamic integration and free energy perturbation.²¹ The free energy difference for transferring a K^+ ion from bulk to the gA center was found to be consistent with that obtained from the 1D-PMF. Because the gA binding site provides a more relevant reference point in the present work, here we perform a similar free energy difference calculation for transferring a K^+ ion from bulk ($z = 20$ Å) to the binding site ($z = 11.3$ Å). The calculations are carried out using the thermodynamic integration method as described in Sec. II. In Fig. 3, we show the running averages of the free energy differences in the forward and reverse directions, and the average of the two. As explained in Sec. II, an intermediate state (W_0) is used in the transformation and the curves labeled K show the $K^+ \rightarrow W_0$ leg of the transformation, and those labeled W show the $W_0 \rightarrow W$ leg. The running averages show that the forward and reverse free energies fluctuate around the average free energies within a 1 kT band as one would expect. Further the average free energies remain stable and have converged to well-defined values. The total free energy change for translocating a K^+ ion from bulk to the binding site is given by the sum of the end points of the solid curves in Fig. 3, which yields $-7.3 + 2.7 = -4.6$ kT. This is in good agreement with -4.5 kT ob-

tained from the 1D-PMF in Fig. 2(b), confirming that the bulk reference value is correctly calculated in the present 1D-PMF calculations.

It is instructive to compare the present K^+ PMF with some of the earlier ones. The central barrier is 21 kT, which is consistent with all other PMF calculations when no correction factors are invoked.^{17–20} The binding sites, however, exhibit differences depending on which gA structure is used. Of the two binding sites at $z=9.6$ and 11.3 Å, we find the outer site deeper with an energy of -4.5 kT. A similar result with a binding energy of -3 kT is obtained in a recent calculation where the 1JNO structure is used.¹⁸ In contrast when the 1MAG structure is employed, the inner binding site comes out deeper with an energy of -7 kT.²⁰ In x-ray diffraction experiments, Tl^+ ions are found to bind at 9.6 Å.⁵¹ NMR experiments, on the other hand, indicate a delocalized binding site for K^+ distributed over the leucine 10–12–14 carbonyl groups,^{52,53} which suggests a broader energy well covering both binding sites. Despite long equilibration times, the PMF's obtained using the 1MAG and 1JNO structures are somewhat different with the former yielding a lower binding energy while the barriers remain the same. After long equilibration, the only important difference that remains between the two structures is the orientation of the Trp9 side chains.³⁸ Thus our results suggest that the Trp9 rotamer state in the 1MAG structure provides a slightly better environment for binding of K^+ ions but does not influence its permeation, consistent with previous observations.⁵⁴

The binding constants of cations with gA have been well determined from NMR experiments, which provide valuable checks on the binding energies obtained from PMF's. We estimate the binding constant of K^+ from the PMF in Fig. 2(b) using Eq. (5). The effective pore radius for a K^+ ion in the binding site is determined from MD simulations as $R \sim 2$ Å, by measuring its radial distribution with respect to the channel axis. Evaluating the integral numerically between ± 15 Å and substituting in Eq. (5), we obtain $K = 1.8 M^{-1}$. The experimental values obtained from NMR are $K = 52.6 M^{-1}$ (Ref. 55), and $60 M^{-1}$,³⁴ which are 30 times larger, indicating a deeper binding site than calculated here. In a similar MD simulation,¹⁸ the K^+ binding constant was estimated as $K = 2.9 M^{-1}$ and agreement with the NMR data of Hinton *et al.*⁵⁵ was claimed, which was quoted as 1.4 – $52.6 M^{-1}$. We note that the NMR data of Hinton *et al.*⁵⁵ are $52.6 M^{-1}$, and the value of $1.4 M^{-1}$ was determined from earlier streaming potential measurements,³¹ which is not as reliable. Also in this estimate of the binding constant,¹⁸ $R = 8$ Å was used for the radius. This is a rather large value and explains how a larger binding constant was obtained in Ref. 18 although the binding site was shallower (-3 kT) than the present PMF (-4.5 kT). To see the effect of a deeper well on the binding constant, we use the PMF in Ref. 20, which has a well depth of -7 kT and yields $K = 17.5 M^{-1}$ —closer to the NMR values. The above examples make the exponential dependence of the binding constant on the well depth very clear and suggest that in order to achieve agreement with the experimental data, a well depth of about -8 kT is required in the K^+ PMF. We remark that the same well depth of -8 kT was obtained when the PMF was obtained from a fit to the

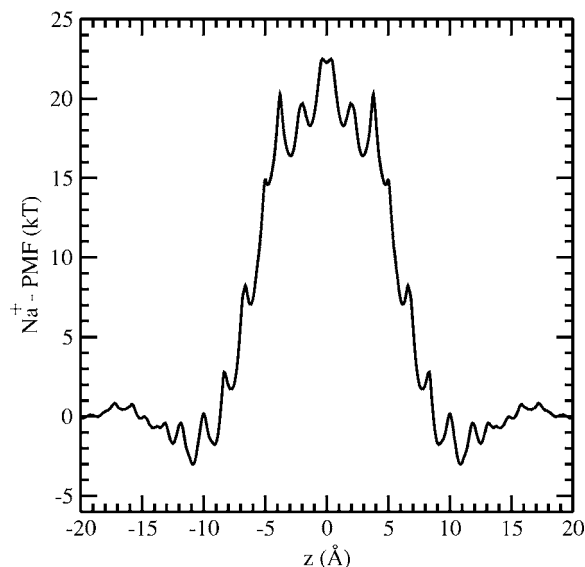


FIG. 4. PMF profile of a Na^+ ion along the central axis of the gramicidin A channel obtained from 1 ns MD simulation for each window using symmetrized ion densities as in Fig. 2(b).

available conductance data for K^+ ions using Brownian dynamics simulations.¹⁵ In this work,¹⁵ the barrier height and well depth in the PMF were treated as parameters, and their optimal values were determined from a best fit to all the available permeation data. Congruence of two completely independent estimates for the binding energy of K^+ gives further confidence on the extracted value of -8 kT.

In Fig. 4, we show the PMF for a single Na^+ ion obtained from a 1 ns MD simulation for each window using the symmetrized ion densities. The basic features of the Na^+ are very similar to that of K^+ shown in Fig. 2(b). The height of the central barrier with respect to the binding site is about 25 kT. Because Na^+ is 0.4 Å smaller, the binding sites are moved further into the channel and appear at $z=9.1$ and 10.9 Å. For the same reason, Na^+ binds to gA in a distinctly off-axis position—about 1.3 Å away from the channel axis on average. The outer binding site is -3 kT deep in energy, slightly less than that of K^+ , while the inner binding site is somewhat better developed compared to that of K^+ . The two binding sites differ in energy by only 1 kT, thus a Na^+ ion can easily hop from one to the other, consistent with the delocalized binding of cations observed in the NMR experiments.^{52,53} These are considerable improvements over the earlier results,^{36,37} where the binding of a Na^+ ion to gA was found to be problematic. To give a more quantitative assessment for the binding energy, we estimate the binding constant of Na^+ ion. The effective radius of Na^+ in the binding site is found to be $R \sim 2.5$ Å. Combining this value with the integral of the PMF in Fig. 4, we obtain for the binding constant of Na^+ , $K = 0.7 M^{-1}$. The experimental values are $K = 36.9 M^{-1}$ (Ref. 55) and $40 M^{-1}$,³⁴ which are 60 times larger. Using the exponential relationship between the binding constant and the well depth as above, we estimate that a well depth of -7 kT is needed in the Na^+ PMF in order to reproduce the experimental data.

We next consider the PMF's for the binding of two ions to gA, which are constructed using several different methods

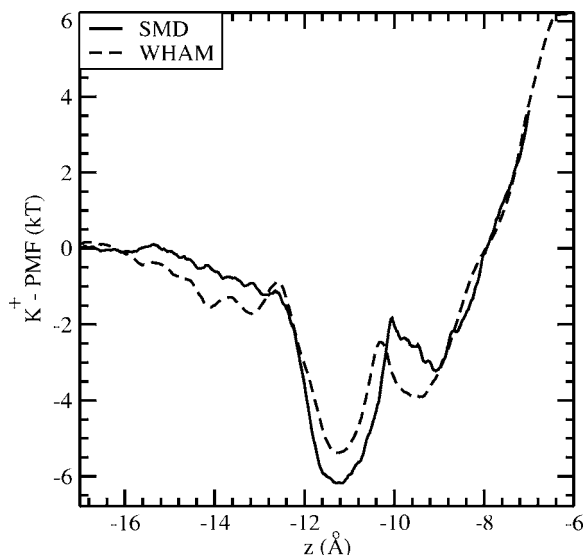


FIG. 5. Comparison of the PMF profile for binding of a single K^+ ion to gA obtained from SMD simulations with that of WHAM [Fig. 2(a)].

as described in Sec. II. Because SMD simulations using Jarzynski's equality are relatively new, we first demonstrate its reliability for determining ionic PMF's in a simple test case that involves binding of a single K^+ ion to gA. In Fig. 5, the PMF obtained from SMD by pulling an external ion to the left-binding site is compared to that obtained from umbrella sampling and WHAM [Fig. 2(a)]. The SMD-PMF closely tracks that of WHAM and reproduces the binding energies within 1 kT, which is within the statistical accuracy of the simulations.

To study double occupancy, we perform a similar set of SMD simulations as above but now with a K^+ ion present in the right-binding site. In Fig. 6(a), we show the positions of the steered and bound ions against the SMD reference point for each of the ten SMD simulations. It is seen that the bound ion leaves the right-binding site in some cases as the steered ion approaches the left site. The PMF obtained from the SMD simulations using Jarzynski's equality is shown in Fig. 6(b) (solid line). In the same plot we also show a similar PMF but obtained using umbrella sampling and WHAM, where a $4 \text{ kT}/\text{\AA}^2$ harmonic restraint is applied on the bound ion (dashed line). There is very little difference between the two PMF's, which indicates that restraining of the bound ion in WHAM did not influence the binding of the second K^+ ion much. The PMF's reveal that the second K^+ ion cannot bind to the usual binding locations at 9.6 and 11.3 \AA but has a shallow (-1 kT deep) binding site around 13 \AA . The binding constant estimated from the PMF is $K=0.1 \text{ M}^{-1}$ while the experimental value determined from NMR is $K=3 \text{ M}^{-1}$.³⁴ Thus the binding constant is overestimated by a factor of 30 as in the case of a single K^+ ion, indicating a similar underestimate of the binding energy by 3–4 kT.

Results of a similar study for the double occupancy of Na^+ ions from SMD simulations are presented in Fig. 7. Positions of the steered and bound ions from ten SMD simulations are shown in Fig. 7(a). In contrast to the K^+ case in Fig. 6(b), here none of the bound Na^+ ions leave the binding site during the steering process, even when the steered ion is

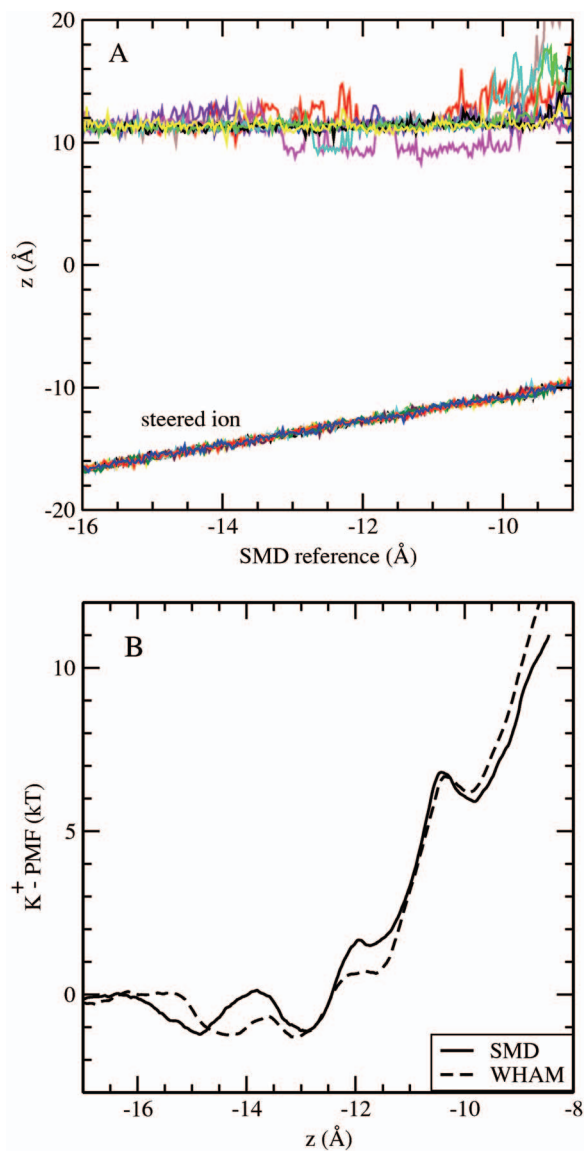


FIG. 6. (Color) SMD simulations for double K^+ occupancy. In (A), the positions of the steered and bound ions are plotted against the SMD reference point for each of the ten SMD simulations. Color is used to help distinguish among different K^+ trajectories; otherwise it has no significance. In (B), we show the PMF profiles of the second K^+ ion determined from the SMD simulations (solid line) and WHAM (dashed line).

moved into the pore beyond the binding site. As explained below, this is due to the off-axis binding of Na^+ ions, which allows exit of pore water without much hindrance. The PMF obtained from the SMD simulations [Fig. 7(b)] shows that the second Na^+ ion binds nearly at the same distance ($z=-11.1 \text{ \AA}$) and with a similar energy (-2.5 kT) as the first one. The PMF yields a binding constant of $K=0.3 \text{ M}^{-1}$, to be compared with the NMR value of $K=4 \text{ M}^{-1}$.³⁴ The reduced discrepancy compared to the binding of a single Na^+ ion is again the result of off-axis binding of Na^+ ions, which unlike in the case of K^+ , does not hinder the binding of a second Na^+ ion.

An alternative way to study double occupancy is to bind the two ions simultaneously in a symmetric fashion as described in Sec. II. The PMF's for simultaneous binding of two K^+ and two Na^+ ions are shown in Fig. 8. As one might

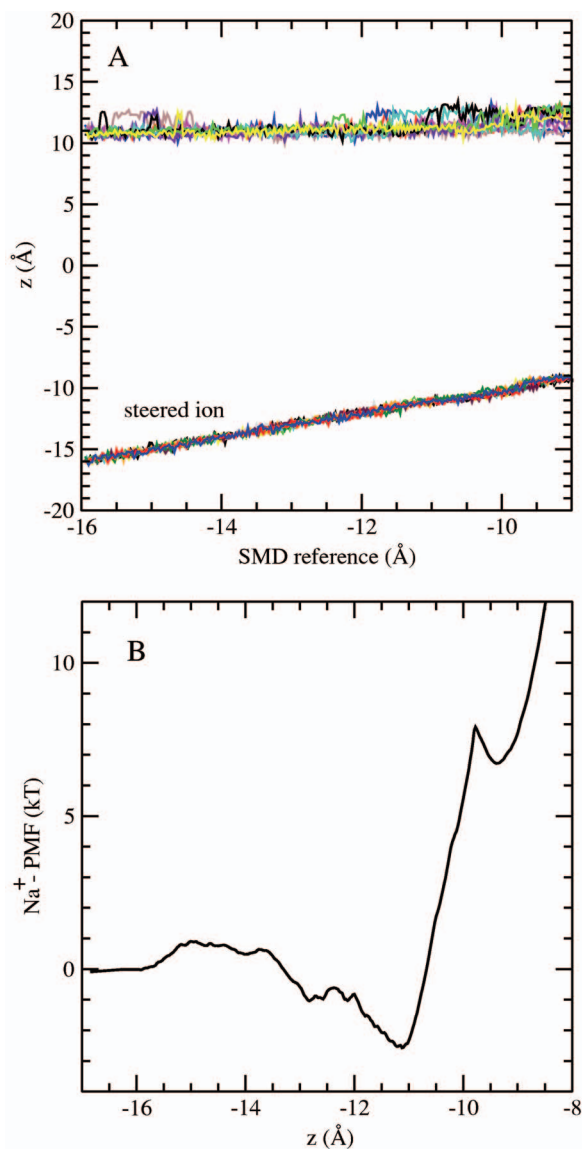


FIG. 7. (Color) Similar to Fig. 6 but for double Na^+ occupancy. In (B) only the SMD result for PMF is shown.

expect, these PMF's are roughly bracketed between those of single and double ion cases. Discussing the K^+ ions first (Fig. 8, solid line), the PMF shows that the two ions can bind to gA simultaneously at $z = \pm 11.5 \text{ \AA}$, slightly further out than that of a single K^+ ion [Fig. 2(b)]. The binding energy is -3 kT , which is in between the single and double ion results. Because this PMF is based on the distance between the two ions, it provides no information on whether the binding occurs in a symmetric fashion or not. PMF's obtained from the individual ion densities—though they do not have a direct physical interpretation—could shed light on this question. From the individual PMF's (not shown), we find that there is a slight asymmetry during the binding of two K^+ ions but once the ions are bound, this asymmetry disappears. When the ions are in the binding sites, there are seven water molecules between them in the channel. One of the water molecules escapes when the ions are pushed to $\pm 10 \text{ \AA}$. Due to single filing in the pore region, water molecules cannot escape when the ions are pushed further in, which leads to a

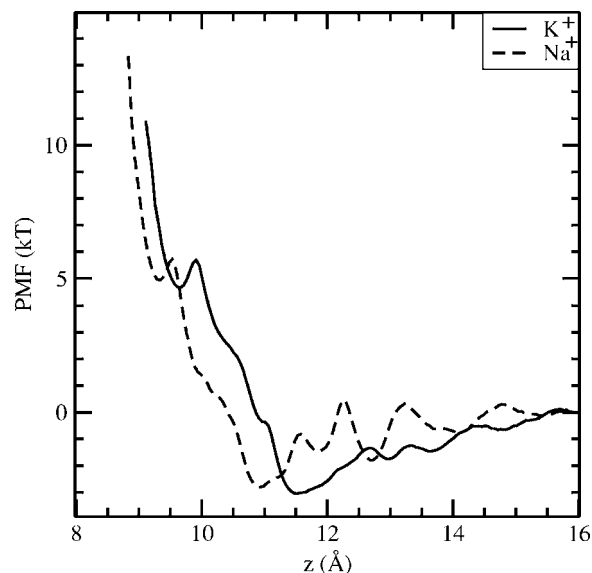


FIG. 8. PMF profiles for simultaneous binding of two K^+ ions (solid line) and two Na^+ ions (dashed line) to gA.

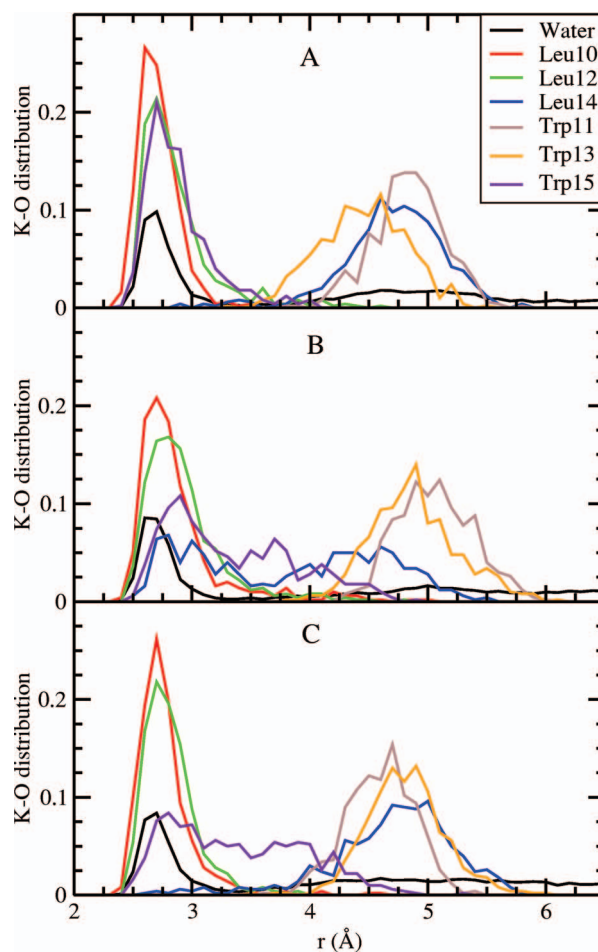


FIG. 9. (Color) Fractional distribution of ion-oxygen distances for the oxygens of water, leucine (10, 12, and 14) and tryptophan (11, 13, and 15), when a single K^+ ion is in the left-binding site (A), and when two K^+ ions are simultaneously bound at the right (B) and left (C) binding sites. In order to have similar scales with the Leu and Trp oxygens, the radial distribution function is shown for water oxygens (i.e., the distribution function is normalized by $4\pi r^2 \Delta r$).

steeply rising PMF after 9 Å. The role of pore water and carbonyl dipoles in the binding process is further discussed below. The PMF for simultaneous binding of two Na⁺ ions (Fig. 8, dashed line) is very similar to those for single and double ion cases—the binding locations and energies are almost the same. Interestingly, the individual PMF's (not shown) exhibit a much larger asymmetry in this case, which arises from different binding configurations of the two Na⁺ ions as discussed further below.

B. Coordination of ions

In order to gain a better understanding of the PMF results, we study how the ions are coordinated in their respective binding sites (Figs. 8 and 9) and the deflections in the orientations of the carbonyl dipoles upon cation binding (Table I). Both K⁺ and Na⁺ ions are coordinated by the neighboring Leu and Trp carbonyl groups and about three water molecules. We find that the Trp9 carbonyl oxygen is located farther than the second hydration shell, and therefore in the following we restrict the carbonyl groups to Leu10, Leu12, and Leu14 and Trp11, Trp13, and Trp15. In Fig. 9, we show the K⁺-O distance distribution for the Leu and Trp oxygens and the radial distribution function (RDF) for the water oxygens (the latter quantity is chosen to prevent the water distribution from dominating the graph). The top part shows the results for a K⁺ ion bound in the left-binding site (A), while the lower two panels show the results for doubly occupied channel with two K⁺ ions simultaneously bound at the right (B) and left (C) binding sites. The average radial distances of the ions from the channel axis are $r=0.4$ Å (A), 1.1 Å (B), and 0.7 Å (C). Thus the K⁺ ions assume a more off-axis position in double occupancy. Integrating the water RDF gives first hydration shells of 3.0 molecules for (A) and 2.75 for (B) and (C), that is, 2 K⁺ ions are slightly less hydrated by water molecules compared to a single K⁺ ion. In all cases, the Leu10 and Leu12 oxygens remain firmly in the

first hydration shell but for the Trp15 oxygen this is true only in the single ion case. In double occupancy, the K⁺ ions are slightly farther away and more off axis, which leads to a broader distribution for the Trp15 oxygen. The other carbonyl oxygens remain mostly in the second shell. One notable exception is the Leu14 oxygen, which is widely distributed in case (B). The K⁺ ion is more off axis in this case, and an examination of the trajectory data shows that it interacts more strongly with the Leu14 oxygen. Inspection of the average dipole deflection angles in Table I provides further evidence for this argument—there is an appreciable deflection of the Leu14 dipole in case (B) compared to the others. The only other appreciable deflection of carbonyl dipoles upon cation binding occurs for Leu12 and Leu12', which range from 11° to 15°. These are larger than the experimental values indicating less than 10° deflection,^{52,53} but the situation gets worse when the K⁺ ion is in the inner binding site²¹ where larger deflections occur.

In Fig. 10, we present a similar study for Na⁺ ions. The average radial distances of the ions from the channel axis are $r=1.3$ Å (A), 1.3 Å (B), and 0.5 Å (C). In double occupancy, the Na⁺ ion on the left side takes a more central position, which leads to it being slightly less well coordinated by the carbonyl groups. In all cases, the integration of the water RDF gives 3.0 molecules in the first hydration shell, so there is no difference between the three cases in that respect. Because the Na⁺ ions are farther in the pore compared to K⁺, the Trp15 oxygen, besides Leu10, remains in the first hydration shell in all cases. We remark that in every case studied, the Leu10 oxygen provides the strongest coordination for the bound cation consistent with the NMR experiments.^{57,58} The hydration shell is completed by the Leu12 oxygen for the ion in the left-binding site (both A and C), which results in a large deflection of the Leu12' dipole (21°–22°) (Table I). The Na⁺ ion on the right side, on the other hand, completes its hydration shell with the Leu14 oxygen, which has to de-

TABLE I. Average deflection angles (in degrees) of the carbonyl dipoles with respect to the channel axis. Negative angle indicates that the dipole is oriented in the opposite ($-z$) direction, e.g., Trp dipoles on the right side and Leu dipoles on the left. The primed residues at the bottom half denote those on the left side of the dimer. The single ions are at the left-binding site ($z \sim -11$ Å). The binding sites for double ions are $z \sim \pm 11.5$ Å for K⁺ and $z \sim \pm 11$ Å for Na⁺. The results with ions in the channel are obtained from 1 ns MD simulations each and those with no ions from 4 ns simulation. The fluctuations in the angles are about 5°–10°.

Residue	No ions	Single ion		Double ions	
		K ⁺	Na ⁺	2K ⁺	2Na ⁺
Leu10	13	22	20	14	23
Leu12	23	17	20	34	14
Leu14	19	16	17	28	54
Trp11	-35	-36	-39	-28	-42
Trp13	-24	-28	-26	-23	-24
Trp15	-39	-46	-42	-48	-52
Leu10'	-17	-13	-23	-21	-28
Leu12'	-14	-29	-35	-28	-36
Leu14'	-22	-14	-11	-15	-14
Trp11'	34	28	28	30	24
Trp13'	35	32	30	34	30
Trp15'	35	36	44	43	46

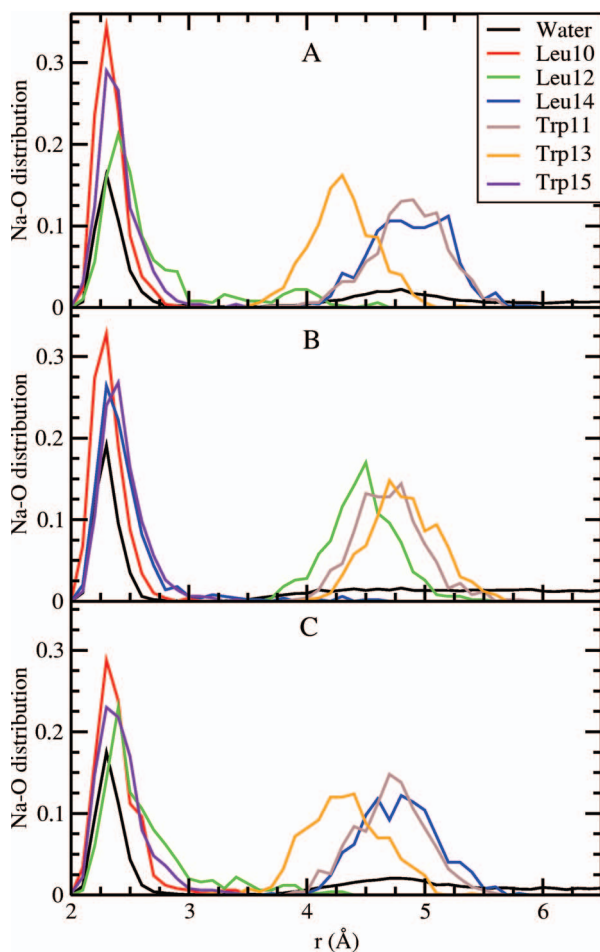


FIG. 10. (Color) Same as Fig. 9 but for Na^+ ions.

fect a considerable amount (35°) to achieve this. As pointed out above, such large deflections of the carbonyl dipoles are not consistent with experiments.^{52,53} The distribution functions in Fig. 10 provide an explanation for the asymmetry of the individual PMF's of Na^+ ions mentioned above. The Leu14 oxygen coordinates the Na^+ ion on the left slightly better than does the Leu12 oxygen the Na^+ ion on the right—the average distances are 2.42 Å in the former and 2.58 Å in the latter. Using these figures to compute the Coulomb interaction between Na^+ and Leu-oxygen yields -7 kT in favor of the Na^+ ion on the right side, which compares favorably with the -5 kT difference found in the binding energies of individual PMF's.

An interesting feature of the gA channel is that the dipoles of water molecules are all aligned along the channel axis with or without an ion in the binding site. When an ion is in the binding site, the water dipoles are clearly aligned along the electric field of the ion but in the absence of an ion, the dipoles can spontaneously flip directions in a subnanosecond time interval.⁵⁶ Simultaneous binding of two cations presents a similar situation, and many such flips of the water dipoles are observed during the construction of the two-ion PMF's. As an example, we show in Fig. 11(a) the time course of the water dipole moments when two cations are bound to the channel symmetrically as in Fig. 8. Of the seven water molecules, dipole moments of 1 or 2 are aligned with

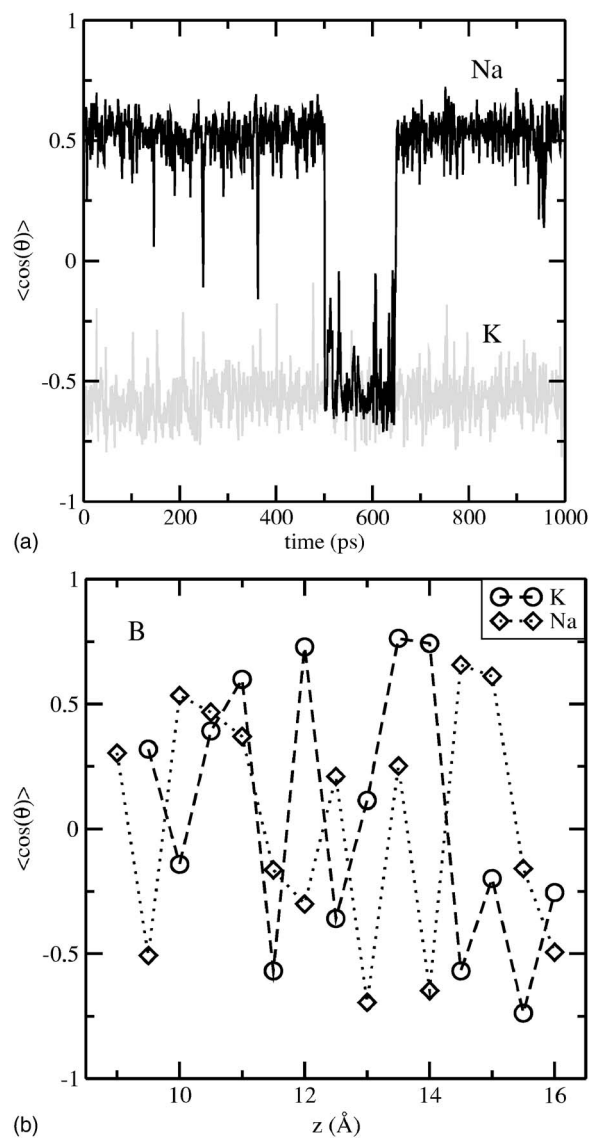


FIG. 11. (A) Time course of the water dipole moment projections to the channel axis (denoted by $\cos \theta$), when two K^+ or two Na^+ ions are simultaneously bound to gA as in Fig. 8. Average of $\cos \theta$ for the seven water molecules in the channel is calculated at each snapshot and plotted against simulation time. (B) The time average of $\langle \cos \theta \rangle$ plotted in (A) is calculated for each PMF window and plotted as a function of the window position.

one ion and the rest with the other one. Thus there is still a net dipole moment associated with the water column in the channel but it is reduced compared to the single ion case. In Fig. 11(a), we show the average of the dipole projections over seven water molecules. For the K^+ ion, the water dipoles remain oriented in the $-z$ direction but in the case of the Na^+ ion, the dipoles are seen to change directions twice in a 0.2 ns interval.

We next address whether the water dipole moments contribute to the asymmetry of the two-ion PMF's. For this purpose, we calculate the time average of $\langle \cos \theta \rangle$ shown in (A) for each PMF window and plot the result as a function of the window position [Fig. 11(b)]. It is seen that even when the ions are away from the binding sites, the average dipole moment of water in the channel is less than the maximal value due to spontaneous flip of the dipoles. As the ions get closer to the binding sites, the net dipole moment of water column

is diminished because of the cancellations. We find no conclusive evidence for correlations between the asymmetries in the PMF's and the average dipole orientations of water in the channel. For example, the largest asymmetry in the individual K^+ PMF's occurs at $z=12.5$ Å, favoring the ion on the right, and the average dipole orientation of water molecules is negative [Fig. 11(b)], which would suggest a correlation between the two quantities. However, in the case of Na^+ PMF's an even larger asymmetry occurs at $z=11$ Å, favoring again the ion on the right but the water dipole moments are oriented in the positive direction in this case. Thus the results of the MD simulations suggest that the water molecules in the channel do not play a significant role in the asymmetric binding of two cations to the channel.

IV. CONCLUSIONS

The present study of single and double ion occupancy in gramicidin A complements our previous work on free energy simulations of ion permeation in gA.^{17,20,21} The previous results for single K^+ PMF's are extended to Na^+ ion and longer simulations are carried out to address the convergence issues. The present results for single cation PMF's indicate that the central barrier of ~ 20 kT (Figs. 1 and 2) is overestimated by about 15 kT compared to the estimates obtained from experimental data.¹⁵ This is a significant discrepancy that would lead to suppression of the channel conductance by many orders of magnitude compared to the experimental values. The most plausible source for the missing stabilization energy for a cation at the center of the channel is the polarization interaction. The force fields currently employed in MD simulations do not incorporate the polarization interaction explicitly but take its effect into account in a mean field approximation by increasing the partial charges on atoms from their gas phase values. Such an approximate treatment of polarization appears to have worked well in bulk water because these force fields have been optimized under bulk conditions. But there is no guarantee that they will work as well in a lipid environment because lipids have very different polarization characteristics compared to bulk water. This expectation is reinforced by a recent semimicroscopic model calculation of the ionic free energies in the gA channel that explicitly included polarization interaction: it has been much more successful in accounting for the ionic free energies compared to the microscopic MD simulations that employed rigid force fields.⁵⁹

The binding constants for single ion occupancy of gA, estimated from the respective PMF's, are one to two orders of magnitude smaller than the experimental values, which suggests that the binding energies are underestimated by 3–4 kT. Similar discrepancies are found for double ion binding to gA. On the positive side, we have shown that double ion binding to gA is energetically feasible, which is an improvement over earlier MD studies that predicted otherwise. Although the problems in binding of cations either singly or doubly are not as severe as translocation problems, they are also harder to rectify because the corrections suggested so far^{18,19} for remedy of the latter have a negligible impact at the binding sites. Again the only obvious source for the miss-

ing binding energy of ions is the polarization interaction, and its explicit inclusion in MD force fields may also help to resolve these discrepancies. We hope that the results documented here and in previous papers will further stimulate construction of polarizable force fields for MD simulations of membrane proteins.

ACKNOWLEDGMENTS

This work was supported by grants from the Australian Research Council. Calculations were carried out using the Barossa cluster at the Australian Center for Advanced Computing and Communications and the SGI Altix cluster at the Supercomputer Facility of the Australian National University.

- ¹D. A. Doyle, J. M. Cabral, R. A. Pfuetzner, A. Kuo, J. M. Gulbis, S. L. Cohen, B. T. Chait, and R. MacKinnon, *Science* **280**, 69 (1998).
- ²J. H. Morais-Cabral, Y. Zhou, and R. MacKinnon, *Nature (London)* **414**, 37 (2001).
- ³Y. Zhou, J. H. Morais-Cabral, A. Kaufman, and R. MacKinnon, *Nature (London)* **414**, 43 (2001).
- ⁴O. S. Andersen and R. E. Koeppe, *Physiol. Rev.* **72**, 89 (1992).
- ⁵B. Hille, *Ionic Channels of Excitable Membranes*, 3rd ed. (Sinauer Associates Inc., Sunderland, MA, 2001).
- ⁶D. W. Urry, *Proc. Natl. Acad. Sci. U.S.A.* **68**, 672 (1971).
- ⁷A. S. Arseniev, I. L. Barsukov, V. F. Bystrov, A. L. Lomize, and Y. A. Ovchinnikov, *FEBS Lett.* **186**, 168 (1985).
- ⁸R. R. Ketchum, W. Hu, and T. A. Cross, *Science* **261**, 1457 (1993).
- ⁹R. R. Ketchum, B. Roux, and T. A. Cross, *Structure (London)* **5**, 1655 (1997).
- ¹⁰L. E. Townsley, A. W. Tucker, S. Sham, and J. F. Hinton, *Biochemistry* **40**, 11676 (2001).
- ¹¹M. B. Partenskii and P. C. Jordan, *Q. Rev. Biophys.* **25**, 477 (1992).
- ¹²B. Roux and M. Karplus, *Annu. Rev. Biophys. Biomol. Struct.* **23**, 731 (1994).
- ¹³S. Kuyucak, O. S. Andersen, and S. H. Chung, *Rep. Prog. Phys.* **64**, 1427 (2001).
- ¹⁴B. Roux, *Acc. Chem. Res.* **35**, 366 (2002).
- ¹⁵S. Edwards, B. Corry, S. Kuyucak, and S. H. Chung, *Biophys. J.* **83**, 1348 (2002).
- ¹⁶P. C. Jordan, *Biophys. J.* **83**, 1235 (2002).
- ¹⁷T. W. Allen, T. Bastug, S. Kuyucak, and S. H. Chung, *Biophys. J.* **84**, 2159 (2003).
- ¹⁸T. W. Allen, O. S. Andersen, and B. Roux, *Proc. Natl. Acad. Sci. U.S.A.* **101**, 117 (2004).
- ¹⁹T. W. Allen, O. S. Andersen, and B. Roux, *Biophys. J.* **90**, 3447 (2006).
- ²⁰T. Bastug, A. Gray-Weale, S. M. Patra, and S. Kuyucak, *Biophys. J.* **90**, 2285 (2006).
- ²¹T. Bastug and S. Kuyucak, *Biophys. J.* **90**, 3941 (2006).
- ²²S. B. Hladky and D. A. Haydon, *Biophys. J.* **73**, 1699 (1997).
- ²³S. B. Hladky and D. A. Haydon, *Biochim. Biophys. Acta* **274**, 294 (1972).
- ²⁴S. B. Hladky and D. A. Haydon, *Curr. Top. Membr. Transp.* **21**, 327 (1984).
- ²⁵E. Neher, J. Sandblom, and G. Eisenman, *J. Membr. Biol.* **40**, 97 (1978).
- ²⁶G. Eisenman, J. Sandblom, and E. Neher, *Biophys. J.* **22**, 307 (1978).
- ²⁷J. Sandblom, G. Eisenman, and J. Hagglund, *J. Membr. Biol.* **71**, 61 (1983).
- ²⁸L. V. Schagina, A. E. Grinlet, and A. A. Lev, *Nature (London)* **273**, 243 (1978).
- ²⁹L. V. Schagina, A. E. Grinlet, and A. A. Lev, *J. Membr. Biol.* **73**, 203 (1983).
- ³⁰B. W. Urban, S. B. Hladky, and D. A. Haydon, *Biochim. Biophys. Acta* **602**, 331 (1980).
- ³¹D. G. Levitt, S. R. Elias, and J. M. Hautman, *Biochim. Biophys. Acta* **512**, 436 (1978).

- ³²P. A. Rosenberg and A. Finkelstein, *J. Gen. Physiol.* **72**, 327 (1978).
- ³³D. W. Urry, T. L. Trapane, C. M. Venkatachalam, and R. B. McMichens, *Methods Enzymol.* **171**, 286 (1989).
- ³⁴N. J. Jing, K. U. Prasad, and D. W. Urry, *Biochim. Biophys. Acta* **1238**, 1 (1995).
- ³⁵S. S. Sung and P. C. Jordan, *J. Phys. Chem.* **92**, 2362 (1988).
- ³⁶B. Roux, B. Prodhom, and M. Karplus, *Biophys. J.* **68**, 876 (1995).
- ³⁷T. B. Woolf and B. Roux, *Biophys. J.* **72**, 1930 (1997).
- ³⁸T. W. Allen, O. S. Andersen, and B. Roux, *J. Am. Chem. Soc.* **125**, 9868 (2003).
- ³⁹W. Humphrey, A. Dalke, and K. Schulten, *J. Mol. Graphics* **14**, 33 (1996).
- ⁴⁰J. F. Nagle and S. Tristram-Nagle, *Biochim. Biophys. Acta* **1469**, 159 (2000).
- ⁴¹T. Bastug, S. M. Patra, and S. Kuyucak, *Chem. Phys. Lipids* **141**, 197 (2006).
- ⁴²L. Kale, R. Skeel, M. Bhandarkar, R. Brunner, A. Gursoy, N. Krawetz, J. Phillips, A. Shinozaki, K. Varadarajan, and K. Schulten, *J. Comput. Phys.* **151**, 283 (1999).
- ⁴³A. D. MacKerell, Jr., D. Bashford, M. Bellott *et al.*, *J. Phys. Chem. B* **102**, 3586 (1998).
- ⁴⁴S. Feller, Y. Zhang, R. Pastor, and B. Brooks, *J. Chem. Phys.* **103**, 4613 (1995).
- ⁴⁵G. M. Torrie and J. P. Valleau, *J. Comput. Phys.* **23**, 187 (1977).
- ⁴⁶S. Kumar, D. Bouzida, R. H. Swensen, P. A. Kollman, and J. M. Rosenberg, *J. Comput. Chem.* **13**, 1011 (1992).
- ⁴⁷C. Jarzynski, *Phys. Rev. Lett.* **78**, 2690 (1997).
- ⁴⁸S. Park and K. Schulten, *J. Chem. Phys.* **120**, 5946 (2004).
- ⁴⁹T. Bastug and S. Kuyucak, *Chem. Phys. Lett.* **425**, 320 (2006).
- ⁵⁰K. A. Duca and P. C. Jordan, *J. Phys. Chem.* **102**, 9127 (1998).
- ⁵¹G. A. Olah, H. W. Huang, W. Liu, and Y. Wu, *J. Mol. Biol.* **218**, 847 (1991).
- ⁵²F. Tian, K. C. Lee, W. Hu, and T. A. Cross, *Biochemistry* **35**, 11959 (1991).
- ⁵³F. Tian and T. A. Cross, *J. Mol. Biol.* **285**, 1993 (1999).
- ⁵⁴A. E. Dorigo, D. G. Anderson, and D. D. Busath, *Biophys. J.* **76**, 1897 (1999).
- ⁵⁵J. F. Hinton, W. L. Whaley, D. Shingu, R. E. Koeppe, and F. S. Milett, *Biophys. J.* **50**, 539 (1986).
- ⁵⁶S. W. Chiu, S. Subramaniam, and E. Jakobsson, *Biophys. J.* **76**, 1939 (1999).
- ⁵⁷R. Smith, D. E. Thomas, A. Atkins, F. Separovic, and B. A. Cornell, *Biochim. Biophys. Acta* **1026**, 161 (1990).
- ⁵⁸F. Separovic, J. Gehrman, T. Milne, B. A. Cornell, S. Y. Lin, and R. Smith, *Biophys. J.* **67**, 1495 (1994).
- ⁵⁹V. L. Dorman and P. C. Jordan, *Biophys. J.* **86**, 3529 (2004).